Received: 27 November 2023 | Revised: 18 January 2024 | Accepted: 11 February 2024

DOI: 10.1111/jeu.13023

Journal of Eukaryotic Microbiology ISOP Published by the International Society of Protistologists

ORIGINAL ARTICLE

Novel cytoskeletal traits in the intestinal parasites (Squirmida, *Platyproteum vivax*) of Pacific peanut worms (Sipuncula, *Phascolosoma agassizii*)

Danja Currie-Olsen[1,2] | **Brian S. Leander**[1]

[1]Department of Zoology, Beaty Biodiversity Research Centre and Museum, University of British Columbia, Vancouver, British Columbia, Canada

[2]Hakai Institute, Heriot Bay, Quadra Island, British Columbia, Canada

Correspondence
Brian S. Leander, Departments of Botany and Zoology, University of British Columbia, 6270 University Blvd., Vancouver, BC V6T 1Z4, Canada.
Email: bleander@mail.ubc.ca

Funding information
Natural Sciences and Engineering Research Council of Canada, Grant/Award Number: 2019-03986

Abstract

The cytoskeletal organization of a squirmid, namely *Platyproteum vivax*, was investigated with confocal laser scanning microscopy (CLSM) to refine inferences about convergent evolution among intestinal parasites of marine invertebrates. *Platyproteum* inhabits Pacific peanut worms (*Phascolosoma agassizii*) and has traits that are similar to other lineages of myzozoan parasites, namely gregarine apicomplexans within *Selenidium*, such as conspicuous feeding stages, called "trophozoites," capable of dynamic undulations. SEM and CLSM of *P. vivax* revealed an inconspicuous flagellar apparatus and a uniform array of longitudinal microtubules organized in bundles (LMBs). Extreme flattening of the trophozoites and a consistently oblique morphology of the anterior end provided a reliable way to distinguish dorsal and ventral surfaces. CLSM revealed a novel system of microtubules oriented in the flattened dorsoventral plane. Most of these dorsoventral microtubule bundles (DVMBs) had a punctate distribution and were evenly spaced along a curved line spanning the longitudinal axis of the trophozoites. This configuration of microtubules is inferred to function in maintaining the flattened shape of the trophozoites and facilitate dynamic undulations. The novel traits in *Platyproteum* are consistent with phylogenomic data showing that this lineage is only distantly related to *Selenidium* and other marine gregarine apicomplexans with dynamic intestinal trophozoites.

KEYWORDS
Apicomplexa, centrin, confocal laser scanning microscopy, microtubules, Myzozoa, *Selenidium*, tubulin

INTRODUCTION

THE Myzozoa is a monophyletic group of primarily single-celled eukaryotes that have adopted diverse modes of nutrition, such as vampire-like predation, photoautotrophy, and parasitism (Cavalier-Smith & Chao, 2004; Leander, 2007; Leander & Keeling, 2003). Most myzozoans fall into two major subgroups, dinozoans and apicomplexans, but several lineages fall outside of these groups, such as chrompodellids/colpodellids and parasitic squirmids (Mathur et al., 2019) (Figure 1). Colpodellids are biflagellated myzocytotic predators of other protozoan predators (e.g. ciliates and *Bodo*) and form an early branching lineage near the origin of apicomplexans (Kuvardina et al., 2002; Leander & Keeling, 2003; Mathur et al., 2019). All members of the Apicomplexa are obligate endoparasites that evolved from a free-living myzocytotic predator

containing a plastid (Cavalier-Smith, 2004; Janouškovec et al., 2015; Leander, 2008b; Leander & Keeling, 2003; Mathur et al., 2019). Among these lineages are important human/animal pathogens, such as *Toxoplasma gondii*, *Plasmodium*, and *Cryptosporidium*. Apicomplexans are characterized by their infective life cycle stage, designated the sporozoite stage, equipped with a host cell invasion apparatus named the apical complex, consisting primarily of a tubulin-based conoid, polar rings and secretory organelles called rhoptries and micronemes (Desportes & Schrével, 2013; Leander & Keeling, 2003; Okamoto & Keeling, 2014; Pacheco et al., 2020; Portman & Šlapeta, 2014). The Squirmida are unusual intestinal parasites of marine invertebrates that form the sister lineage to the clade consisting of chrompodellids/colpodellids and apicomplexans (Leander, 2006, 2008a; Rueckert & Leander, 2009) (Figure 1). Further investigation of early diverging myzozoans, such as squirmids, will provide important insights into the unity and diversity of the group, including novel cases of convergent evolution at the ultrastructural and behavioral levels (Leander, 2008a).

Squirmids are similar to gregarine apicomplexans (Leander, 2006, 2008a, 2008b; Leander et al., 2003; Mathur et al., 2019; Rueckert & Leander, 2009; Yokouchi et al., 2022). Gregarines have a conspicuous haploid feeding stage called a "trophozoite" that inhabits extracellular spaces of their invertebrate hosts, such as the intestinal lumen, coelom, and reproductive vesicles. Trophozoites exhibit exceptional diversity of sizes and shapes across various lineages, ranging from 20 to over 1000 μm long, and have a modified apical end that functions as an attachment apparatus (Desportes & Schrével, 2013; Leander, 2006, 2008b). These feeding cells tend to have hundreds of densely packed longitudinal epicytic folds that increase surface area for acquiring nutrients within the host intestine (Leander, 2008b). However, *Selenidium* is a lineage of gregarines found exclusively in marine invertebrates and with trophozoites that have retained several ancestral traits, such as vermiform cell shapes, dynamic undulations, a myzocytosis-based mode of feeding and relatively few epicytic longitudinal folds (<50) (Leander, 2007, 2008b; Leander et al., 2003; Wakeman & Horiguchi, 2018). The trophozoites of *Selenidium* tend to have transverse striations on the cell surface associated with a dense layer of longitudinally arranged microtubules subtending the plasma

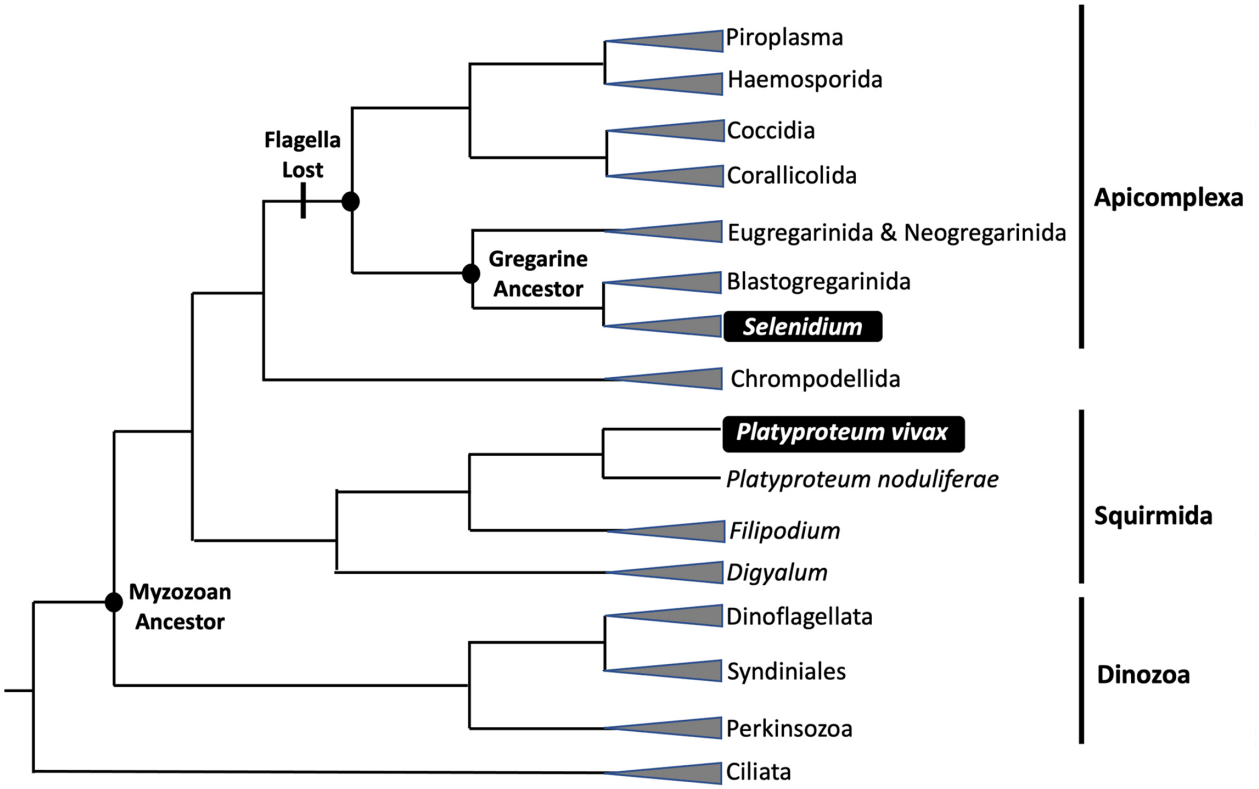

FIGURE 1 Synthetic tree reflecting the current phylogenetic framework of myzozoans (ciliates included as the outgroup). The tree shows that the Squirmida (*Platyproteum* spp., *Filipodium*, and *Digyalum*) branch separately from gregarines and form the sister lineage to a clade consisting of apicomplexans and chrompodellids. The myzozoan ancestor is inferred to have been a biflagellated, myzocytotic-feeding predator. Parasitism evolved independently multiple times within the Myzozoa, and flagella were lost in the most recent ancestor of apicomplexans in association with the origin of parasitism. The phylogenetic positions of the specific lineage investigated in this study, namely *Platyproteum vivax*, and the lineage of gregarine apicomplexans that most closely resembles *Platyproteum*, namely *Selenidium*, are indicated with black boxes.

membrane that generate dynamic bending and twisting movements (Leander, 2006, 2007; Leander et al., 2003; Rueckert & Leander, 2009; Wakeman, Heintzelman, & Leander, 2014). Most other gregarines do not have a dense layer of microtubules below the plasma membrane and instead have relatively rigid trophozoites that use gliding motility (Leander, 2008b).

The Squirmida as represented by *Platyproteum vivax*

Platyproteum vivax inhabits the intestinal tract of the Pacific peanut worm *Phascolosoma agassizii* and was originally described as *Selenidium vivax* without any supporting light micrographs or molecular phylogenetic data (Gunderson & Small, 1986). *Platyproteum vivax* was previously considered to be a member of *Selenidium* because the trophozoite was found in the intestinal lumen of a marine worm, could grow to large lengths (up to 550 μm), and displayed highly dynamic twisting movements (Gunderson & Small, 1986). It was also noted that *P. vivax* had transverse striations and some transient longitudinal surface folds that resembled the transverse striations and relatively few permanent longitudinal epicytic folds of *Selenidium* species (Gunderson & Small, 1986; Leander, 2006; Leander et al., 2003).

The first molecular phylogenetic analyses of *P. vivax* using SSU rDNA sequences showed that this species branched in an unresolved position near the origin of the Myzozoa (Leander et al., 2003). This intriguing phylogenetic position motivated a relatively comprehensive ultrastructural study of *P. vivax* using scanning electron microscopy (SEM), transmission electron microscopy (TEM) and videography of cell movement patterns (Leander, 2006). TEM data revealed that *P. vivax* possessed a dense layer of longitudinal microtubules, similar to *Selenidium* (Leander, 2006, 2008b). However, it was also noted that the trophozoites of *P. vivax* displayed extreme flattening and folding movements, distinct from the twisting and undulating motion of *Selenidium* (Leander, 2006). Additional SSU rDNA sequences were then obtained from several species of *Selenidium* and another unusual intestinal parasite of sipunculids, namely *Filipodium phascolosomae* (Rueckert & Leander, 2009). Molecular phylogenetic analyses of these data showed that a distinct clade consisting of *P. vivax* (ex. *Selenidium vivax*) and *F. phascolosoma* did not branch closely with any of the *Selenidium* lineages in the analysis (Rueckert & Leander, 2009). This molecular phylogenetic context combined with the distinct ultrastructural traits of *P. vivax* justified the removal of *P. vivax* from *Selenidium* and the establishment of a new genus, *Platyproteum* (Rueckert & Leander, 2009). The clade consisting of *Platyproteum* and the co-infecting species *F. phascolosoma* were then reassigned to a novel taxon, the Squirmida (Cavalier-Smith, 2014). Molecular phylogenetic analyses of multiple gene sequences from transcriptomic data confirmed that squirmids (i.e. *Platyproteum* and *Filipodium*) branch separately from gregarines and form the sister lineage to a clade consisting of apicomplexans and chrompodellids (Mathur et al., 2019) (Figure 1). Therefore, gregarine-like traits in members of the Squirmida, like *Platyproteum*, unexpectedly reflect convergent evolution, and further investigation into the details of their ultrastructural organization is expected to reveal novel differences associated with these independent evolutionary histories.

Cytoskeletal traits reflect phylogeny

Components of the cytoskeleton form some of the most important structures in myzozoans, such as the apical complex in apicomplexans, and variations in their organization reflect phylogenetic relationships. For instance, intracellular apicomplexan parasites, like *Toxoplasma gondii* and *Plasmodium*, have a specific number of subpellicular microtubules that organize the cell shape and radiate down from the apical complex, tapering off just before the posterior end (Francia et al., 2015; Morrissette et al., 1997). This arrangement allows for effective alterations of the cell shape for host cell penetration. Residing between the plasma membrane and the inner membrane complex is a system composed of myosin, associated myosin-gliding proteins, and multiple-membrane spanning proteins, collectively referred to as the glideosome system (Bullen et al., 2009; Frénal et al., 2017; Heintzelman, 2015). Most species of gregarines do not have dense layers of cortical microtubules and utilize the actin-myosin system of the cytoskeleton to generate gliding movements (Heintzelman, 2004, 2015). By contrast, *Selenidium* and *Platyproteum* rely on a dense layer of cortical microtubules to generate undulating movements (Leander, 2006, 2008a, 2008b; Yokouchi et al., 2022). Examination of these cytoskeletal components with immunofluorescence and confocal laser scanning microscopy (CLSM) is a powerful way to reconstruct their three-dimensional organization to better infer function (Heintzelman, 2004, 2015). These data will also allow for comparisons of the cytoskeletal systems in squirmids, gregarine apicomplexans, and other lineages of myzozoans to reconstruct patterns of evolution that reflect specific parasitic lifestyles (e.g. intestinal parasitism).

The microtubular cytoskeleton of most eukaryotic lineages is anchored by a system of components usually consisting of two basal bodies, interconnected microtubular roots, and a surrounding matrix of associated proteins (e.g. gamma tubulin and centrin), collectively called the flagellar apparatus, that functions

as the microtubule organizing center (MTOC) for the cell (Moestrup, 2000; Yubuki & Leander, 2013). Although the fundamental components of MTOCs are conserved, variations in these structures are phylogenetically informative at the deepest levels in the tree of eukaryotes (Moestrup, 2000; Yubuki et al., 2016; Yubuki & Leander, 2013). In free-living single-celled eukaryotes, basal bodies are usually arranged in pairs, positioned near the cell surface, and anchor the 9+2 arrangement of microtubules within the axoneme of a flagellum (Beisson & Wright, 2003; Kilburn & Winey, 2008; Marshall, 2008). Basal bodies are a crucial structure of the cytoskeleton as they mediate the organization and coordination of the cytoskeletal elements utilized for motility and mitosis. Investigation of these structures in early-diverging myzozoans is expected to reveal important insights regarding the evolution of cytoskeletal organization within the group and beyond (Okamoto & Keeling, 2014). In fact, the intestinal trophozoites of a new species of *Platyproteum* recently reported from Japan, namely *P. noduliferae* were unexpectedly shown to possess a pair of inconspicuous flagella (Yokouchi et al., 2022).

The calcium-binding protein centrin is essential for the structure and function of the MTOC (Beisson & Wright, 2003). Although centrin was originally described as a protein that was associated with the basal bodies of the unicellular alga, *Chlamydomonas reinhardtii* (Salisbury et al., 1984), it has since been associated with function of MTOCs across the tree of eukaryotes (e.g. *Paramecium*, *Chlamydomonas*, and yeast) (Beisson et al., 2001; Klotz et al., 1997; Ruiz et al., 2005; Salisbury, 1995). However, only a few studies of species within the Myzozoa have investigated the involvement and localization of centrin in the MTOC, and these are limited to dinoflagellates; in these species, centrin is associated with "collars" located at the proximal end of the basal bodies and with fibers that connect the basal bodies together to form the MTOC (Beech et al., 1991; Höhfeld et al., 1994; Roberts & Roberts, 1991). Visualization of centrin localization with CLSM in other lineages of myzozoans will provide context for understanding how centrin-based structures have either been lost or diversified over time.

Phylogenomic data have shown that there have been multiple independent transitions from free-living to parasitic modes of nutrition within the Myzozoa (Janouškovec et al., 2019; Mathur et al., 2019; Moore et al., 2008; Mylnikov, 2009; Yokouchi et al., 2022). The trophozoites of *Platyproteum* are similar in morphology, behavior, habitat, and host affinity to the trophozoites of *Selenidium*, so much so that *P. vivax* was originally classified within *Selenidium*. The goal of this study is to characterize the cytoskeletal organization (e.g. tubulin, centrin) of squirmids, as represented by *P. vivax*, using CLSM in order to identify novel traits and fundamental differences with gregarine apicomplexans that reflect the independent origins of intestinal parasitism.

MATERIALS AND METHODS

Collection of hosts and isolation of *Platyproteum vivax*

Individuals of the sipunculid *Phascolosoma agassizii* (Keferstein, 1967) were collected at low tide (0.8–1.0 m above Canadian Chart Datum) from the rocky intertidal zone of Grappler Inlet near the Bamfield Marine Sciences Centre in Bamfield, BC (48.838239, −125.133946) in April of 2022, and from the intertidal zone of Whiffin Spit, Sooke, BC (48.356404, −123.726090) in August and October of 2022. Hosts were transported to the University of British Columbia (UBC) in containers with seawater aerated with portable air pumps (Zyyini cat# B07T6ZMFLG) in a cooler. In the laboratory, *P. agassizii* were stored in a recirculating sea table kept at 10°C and a salinity of 34 PSU. The host worms were dissected using fine tip scissors to cut through the thick epidermis, along with pins and forceps to help isolate their intestinal tract. Depression microscope slides filled with cold filtered seawater and fine tip forceps were used to dissect the intestinal tract to release the gut contents onto the slide. Depression slides were then placed on an inverted microscope to locate trophozoites. Trophozoites conforming to the description of *P. vivax* were isolated from the gut contents using glass pipette micromanipulation and were washed twice in filtered seawater. The isolated trophozoites were then prepared for DIC, LM, SEM, and CLSM.

Light microscopy

Differential Interference Contrast images were taken using a Zeiss Axioplan 2 microscope equipped with a Zeiss-Axiocam 503-color camera. Live trophozoites were isolated and placed on a microscope slide with a drop of cold filtered seawater. A 1.5-mm thick, 20 × 20 mm coverslip with a Vaseline coating around the edges was gently placed on top of the specimens. Images of the trophozoites were then taken using the DIC setting on the Zeiss Axioplan 2 microscope.

Scanning electron microscopy

Using a glass micropipette, isolated trophozoites were placed into the threaded hole of a Swinnex filter holder, containing a 10-μm polycarbonate membrane filter (Milipore Sigma, cat #: TCTP04700), submerged in seawater within a cylindrical film canister (5 cm

tall, 3 cm diameter). The base of a 50-mL glass beaker was covered with Whatman filter paper and saturated with 4% Osmium tetroxide (OsO_4). The trophozoites were fixed with OsO_4 vapors for 10 min by placing the beaker over the canister. Following vapor fixation, six drops of 4% OsO_4 were added directly to the seawater in the Swinnex filter holder and the trophozoites were fixed for an additional 10 min. A 10-mL syringe filled with distilled water was screwed to the Swinnex filter holder while in the canister. The entire apparatus (filter holder + syringe) was then removed from the film canister containing seawater and fixative and the trophozoites were washed with distilled water two times to remove host debris and salt granules from seawater, using a syringe and plunger which screwed to the filter holder. Following distilled water wash, the trophozoites were dehydrated with a graded series of ethyl alcohol beginning at 30% ethanol, with 10% incremental increases. Additional sample preparation was done in the bioimaging facility, where specimens were critical point dried with carbon dioxide using the Tousimis Autosamdri 815B Critical Point Dryer. Filters were then mounted on stubs using carbon double-sided tape, and sputter coated with gold palladium using the Cressington 208HR Resolution Sputter Coater and visualized using the Hitachi S2600 Scanning Electron Microscope.

Tubulin staining

The tubulin staining protocol used is derived from Angel et al. (2021). Isolated trophozoites were placed in the chambers of 8-well removable silicon chamber slides (ibidi, cat# 80841) coated with 0.1% poly-L-lysine (Ted Pella Inc. cat# 18026) and contained 4% paraformaldehyde (PFA) and filtered seawater. The trophozoites were fixed in PFA in a fume hood for 20 min. After fixation, each chamber was washed three times with 10% phosphate-buffered solution (PBS) for 10 min each at room temperature (hereafter, washed for 30 min). After the final PBS wash, the specimens were incubated in a blocking solution containing 10% PBS Triton™ X-100 0.2% (PBT, Millipore Sigma, cat # T9284) and 5% bovine serum albumin (BSA, Sigma-Aldrich, cat # A9418) at room temperature for 30 min. The specimens were then treated with mouse anti-acetylated alpha tubulin (Sigma-Aldrich, cat# T6793) at a concentration of 1:100 in blocking solution (same as described above) overnight in a 4°C chamber. After incubation, the primary antibodies were removed with three 10-min washes of 10% PBT at room temperature. The cells were then treated with a fluorescently tagged secondary antibody mix consisting of donkey-antimouse Alexa Fluor 647 (Invitrogen, cat# A31571) at a concentration of 1:100 at room temperature for 3 h. Secondary antibodies were removed with three washes of 10% PBT (10% PBS + 0.2% TritonTM X-100) at room temperature.

Centrin staining

The centrin staining protocol used is derived from the protocol used in Wakeman, Heintzelman, and Leander (2014). Although the protocol was very similar to the tubulin staining, the key differences are highlighted here. For centrin labeling, specimens were fixed (4% PFA + 10% PBS + 50 mM of egtazic acid) and washed for 30 min with PBT-EGTA (10% PBT + 50 mM of egtazic acid). This protocol utilized a more aggressive permeabilization step. A permeabilization buffer (15% PBT + 63 mM EGTA +5% BSA) was prepared and trophozoites were permeabilized for 1 h after the PFA washes were completed. Following permeabilization, specimens were incubated with the primary antibodies rabbit anti-centrin (Sigma-Aldrich, cat# ABE480) at a concentration of 1:100 in a blocking solution (20% PBT + 50 mM of EGTA +5% BSA) overnight at 4°C. After incubation, the primary antibodies were removed with multiple washes of PBT-EGTA at room temperature for 30 min. The cells were then incubated in the dark with a fluorescently tagged secondary antibody mix consisting of goat anti-rabbit Alexa Fluor 488 (Invitrogen, cat# A11070) at a concentration of 1:100 at room temperature for 3 h. Stained specimens were washed with three exchanges of 10% PBT-EGTA at room temperature.

Slide mounting

Following the secondary antibody incubation, the silicon chambers were removed by peeling them off using fine forceps. Cityfluor mounting media (Electron Microscopy Science, cat# 17970-25) was then placed on both the slide and on a 1.5-mm thick 20 × 20 mm coverslip. The slide containing the specimens was carefully covered with the coverslip using fine forceps. Excess moisture was removed using strips of Whatman filter paper which were placed at the edge of the coverslip to collect moisture. The coverslip was then sealed onto the slide using nail polish. The slides were kept in a dark, dry space to avoid photobleaching until imaging.

Controls

For each centrin and tubulin staining trial, a control slide containing specimens only fixed in PFA (PFA with EGTA for centrin protocol) and a negative control slide containing fixed specimens only treated with the fluorescently tagged secondary antibodies (to ensure that nonspecific binding was not occurring) were visualized using the same settings on the Olympus FV1000 confocal

scope. The control and negative control slides were also verified for autofluorescence using the Olympus BX53 light/fluorescence microscope at the UBC Bioimaging Facility. No significant patterns of autofluorescence were detected.

CLSM image capture

CLSM data for all slides (control, negative control, and treatment groups) were captured with the Olympus FV1000 CLSM scope with 20× and 40× magnification lens (40× with water immersion, Numerical Aperture (NA): 1.10) at the UBC Bioimaging Facility. Visualization was performed with excitation lasers of wavelength 473 and 635 nm to excite Alexa 488 (centrin, recommended excitation wavelength: 498/520 nm) and Alexa 647 (tubulin, recommended excitation wavelength: 648/670 nm) fluorescent molecules (tagged onto secondary antibodies), respectively. Images were taken using Olympus Fluoview software (FV10-ASW2) operated by Windows 7.

MitoTracker procedure

To visualize mitochondria in *P. vivax*, a protocol was derived to treat live cells with a fluorescently labeled MitoTracker dye which functions by using the mitochondrial membrane potential. Live trophozoites were placed in removable silicon chamber slides containing chilled, filtered seawater. A 1-mM stock solution of MitoTracker™ Green (Thermo Fisher, cat# M7514) was prepared. Chamber slides were then filled with MitoTracker treatment solution containing 400-nM MitoTracker™ Green, 10% PBS, and 2.5% BSA. Cells were incubated in solution for 30 min in a 4°C refrigerator. Following incubation, two 10-min washes with chilled, filtered seawater were performed. After washing, the silicon chambers of the slide were gently removed using fine forceps and 5 µL of SlowFade™ Diamond Antifade Mountant (Thermo Fisher, cat # S36968) was placed on the slide containing the live trophozoites, and on a 1.5-mm thick 60 × 20 mm coverslip. The coverslip was placed on top of the remaining liquid containing the trophozoites. A small amount of excess moisture was gently removed using Whatman filter paper. The slides were kept in a small Styrofoam cooler with ice while being carefully transported to the UBC Bioimaging Facility for visualization on the Olympus FV1000 CLSM scope with a 20× magnification lens with water immersion. Visualization was performed with an excitation laser of 473 nm to excite MitoTracker Green (recommended excitation wavelength: 490/516 nm). Images were taken using Olympus Fluoview software (FV10-ASW2) operated by Windows 7. A control slide with live specimens which were not treated with MitoTracker was also visualized under the same settings as the treatment slide and was verified for autofluorescence under the BX53 fluorescence microscope; no significant patterns of autofluorescence were detected.

Actin staining

Phalloidin staining was attempted on the trophozoites of *P. vivax*. Two main protocols were tested with several attempted trials and various alterations of the concentrations. Isolated trophozoites were placed in a chamber slide and fixed using 4% PFA in seawater buffer for 20 min at room temperature. Following fixation, a 30-min PBS wash was conducted. Attempts were made with two different phalloidin products one was Alexa Fluor 405 Phalloidin (Thermo Fisher cat # A30104) and the other was the Alexa Fluor 647 Phalloidin (Thermo Fisher cat# A22287). After fixation, a 100-nM phalloidin solution in PBS buffer was added to the chamber slide and cells were incubated for 30 min. Several different trials were conducted where the concentration of phalloidin and the incubation times were altered (200, 250, 300, 400, and 500 nM concentrations were attempted, and incubation times ranging from 1 h to overnight were tested). A different protocol was also tested whereby a permeabilization step was included, using the same permeabilization buffer as described for the centrin staining. This protocol also utilized EGTA in the fixation and washing buffers, at the same concentrations as described above.

After phalloidin incubation, the phalloidin solution was removed and a two 20-min PBS washes were conducted at room temperature for both protocols. Silicon chambers were then removed, and slides were mounted with cityfluor media and sealed using nail polish. Imaging was performed at the UBC Bioimaging Facility using the Olympus FV1000 confocal laser scanning microscope with a 40× magnification lens with water immersion (NA: 1.10). Visualization was performed with an excitation laser of wavelength 405 nm (phalloidin, recommended excitation wavelength: 405/450 nm) and 635 nm (phalloidin, recommended excitation wavelength: 650/668 nm) to excite Alexa 405 and 647, respectively. Images were taken using Olympus Fluoview software (FV10-ASW2) operated by Windows 7. A control slide with specimens fixed in PFA (and not treated with MitoTracker) was also visualized under the same settings as the treatment slide and was verified for autofluorescence under the BX53 Fluorescence Microscope, no significant patterns of autofluorescence were detected.

Image processing

Images were processed and edited using cyberduck, cellSens, and Fiji, version 2.00 (Wayne Rasband, National Institute of Health). Fiji was used to take measurements of cells and organelles.

RESULTS

General morphology of the trophozoites

Trophozoite shape and movement was consistent with descriptions provided by Leander (2006). Trophozoites are flattened and display highly dynamic peristaltic movement with the cell shape changing constantly (Figures 2 and 3). The size of the trophozoites observed varied considerably, with fully elongated cells as long as 510 µm (Figure 2A) and some contracted cells as small as 40 µm long (Figure 3A). The relaxed cell shape (not completely contracted or completely elongated) averaged 230.5 ± 26.9 µm (mean ± SE; $n = 15$) long. DIC images revealed a relatively large nucleus ranging from 13 to 40 µm in diameter and located in the middle of the cell ($n = 13$, Figure 2); the nucleus was shaped like a flattened oval and often contained a conspicuous nucleolus. SEM revealed surface patterns consisting of transient longitudinal ridges and arrays of transverse (i.e. circumferential) striations arranged in clusters across the entire trophozoite (Figure 3). Transverse striations were present in higher numbers in areas of the cell where the trophozoite was more contracted (Figure 3).

The anterior end of the trophozoites took on the form of an oblique straight-edge, termed the "anterior apparatus" in this study, that is analogous to the host attachment end in gregarines apicomplexans (i.e. the mucron) (Figures 2 and 3). Like the rest of the trophozoite, the anterior apparatus took on a range of shapes during continuous peristaltic-like movements. Nonetheless, the angle of the oblique straight-edge reflected the two different sides of the flattened trophozoites; we arbitrarily designated the "dorsal side" as visible when the anterior apparatus is oriented to the right, and the "ventral side" as visible when the anterior apparatus is oriented to the left. DIC light micrographs and SEM revealed the presence of two flagella protruding from the anterior apparatus (Figures 2 and 3). The flagella were 6–9 µm long and were constantly in motion in living cells.

Localization of centrin

Centrin staining revealed two distinct bodies positioned below the plasma membrane along the elongated edge of the anterior apparatus (Figure 4). The distance between the two centrin-stained bodies was approximately 10 µm. The exact positions of the two centrin-stained bodies along the anterior apparatus varied slightly between the trophozoites observed;

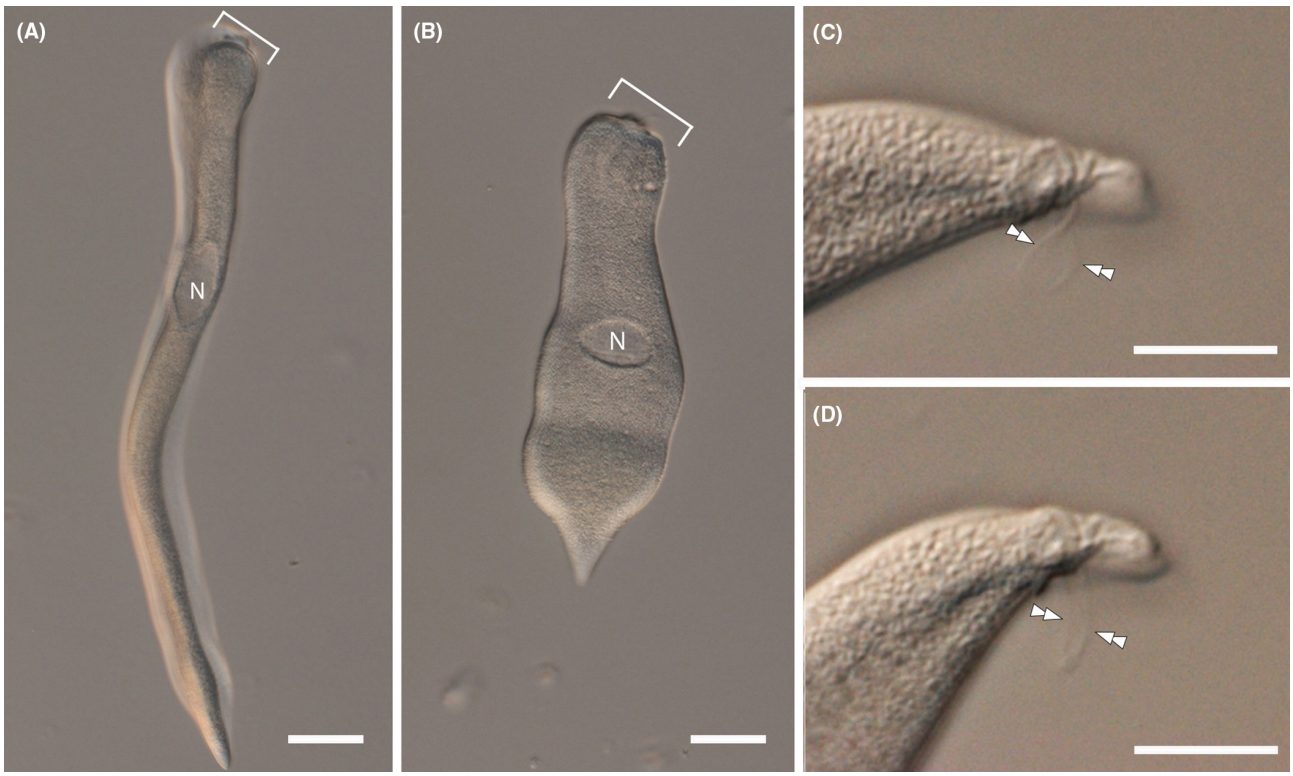

FIGURE 2 Differential interference contrast (DIC) light micrographs of living trophozoites of *Platyproteum vivax* showing general morphology. (A) An elongated trophozoite viewed from the lateral edge showing the flatness of the cell, the anterior apparatus (bracket) and the flattened nucleus (N). (B) A semi-contracted trophozoite showing the anterior apparatus oriented to the right (bracket), the dorsal surface of the cell, and the central position of the oval nucleus (N). (C, D) High magnification views of the anterior end of a cell showing the presence of two short flagella (double arrowheads). Scale bars: A, B = 50 µm; C, D = 10 µm.

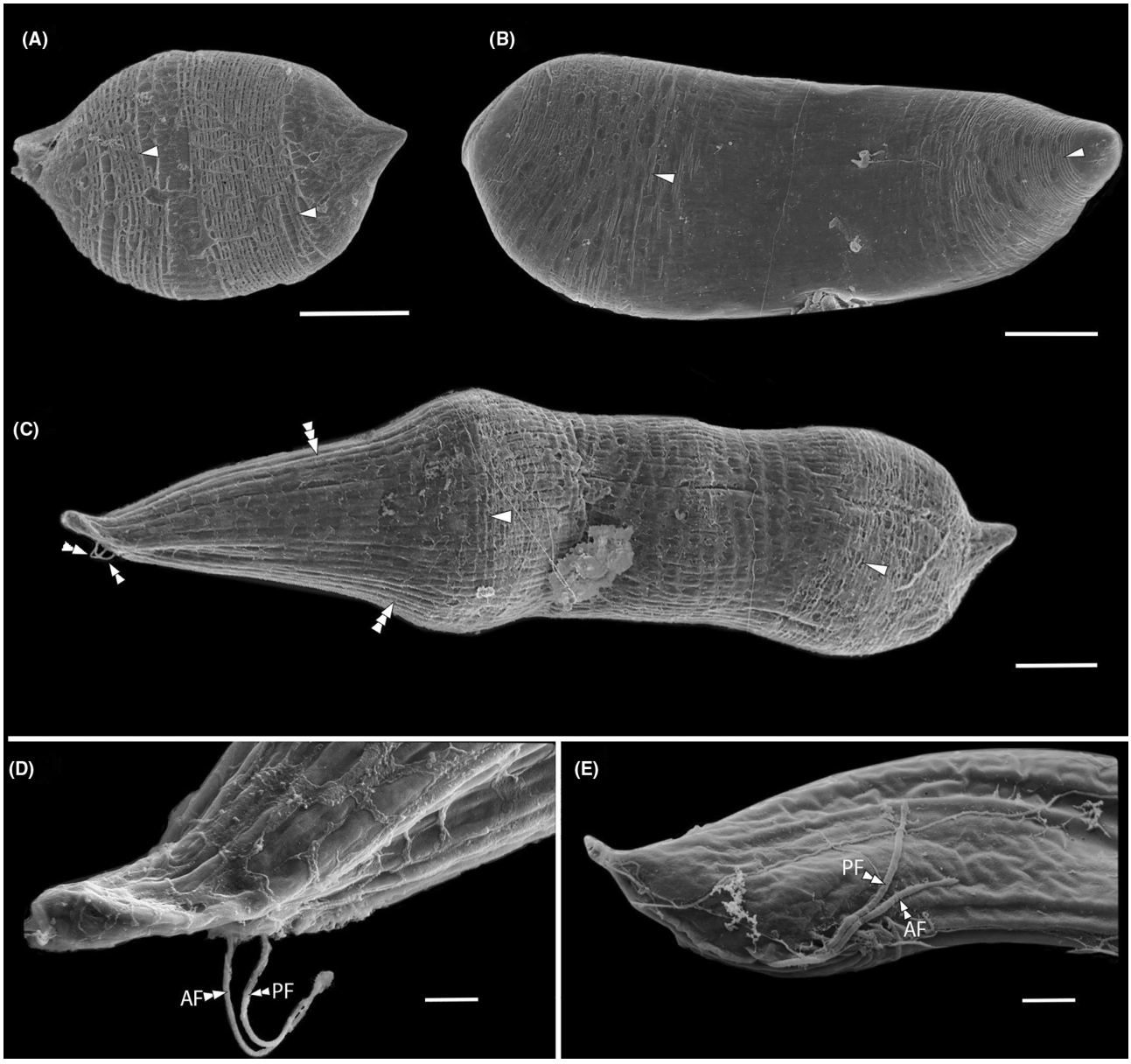

FIGURE 3 Scanning electron micrographs (SEM) of the trophozoites in *Platyproteum vivax*. (A–C) Trophozoites representing different stages of movement showing the anterior end oriented to the left, longitudinal surface folds (triple overhead arrows), transverse surface folds (arrowheads), and two relatively short flagella (double arrowheads). (D, E) High magnification SEMs of the anterior apparatus showing the emergence of an anterior flagellum (AF) and a posterior flagellum (PF). Scale bars: A–C = 10 μm B, D and E = 2 μm.

however, there was always one body that was closer to the anterior-most tip of the anterior apparatus. The positions of the centrin-stained bodies were consistent with the positions of the two flagella observed with LM and SEM (Figures 2 and 3).

Localization of tubulin

Fluorescent visualization of alpha tubulin staining on the cell surface focal plane revealed longitudinal striations of microtubules running along the entire length of the trophozoites, termed "longitudinal microtubule bundles" (LMBs) (Figure 5). Fluorescence was consistently pronounced along the periphery of the trophozoites regardless of the focal plane. Images taken at deeper focal planes of the trophozoites did not show longitudinal striations of microtubules other than the tubulin localized to the exterior edge of the cell (Figure 6). Comparison of the images from the superficial focal planes and deeper focal planes confirms that the tubulin was localized in longitudinal bundles positioned just below the entire outer membrane complex of the cell (Figures 5 and 6).

Tubulin staining also revealed an unexpected, curved row of evenly spaced points, which extended along the

Journal of Eukaryotic Microbiology ISOP Published by the International Society of Protistologists

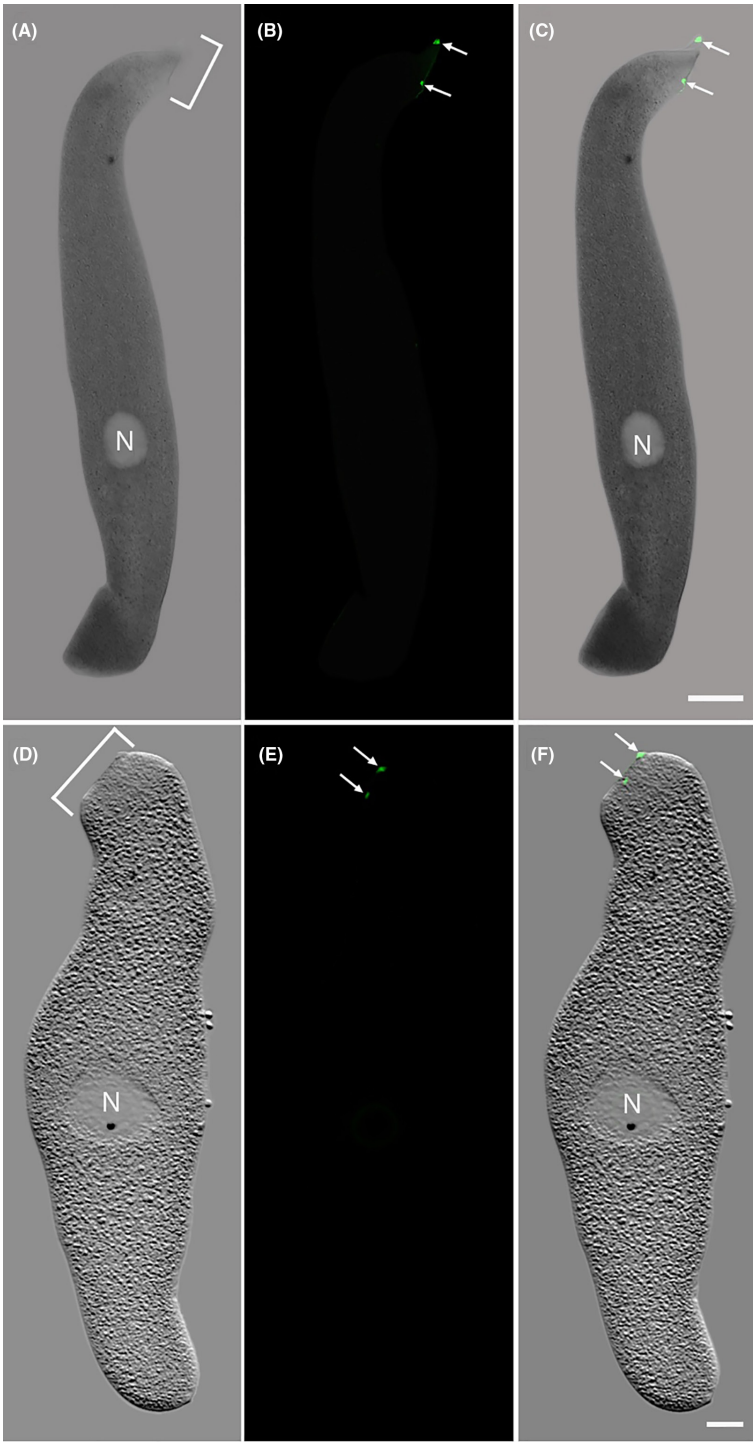

FIGURE 4 Differential interference contrast (DIC) and confocal laser scanning micrographs (CLSM) showing two different trophozoites of *Platyproteum vivax* stained for centrin (green). (A) DIC image showing the central nucleus (N) and the dorsal side of the cell as indicated by the anterior apparatus (bracket) oriented upwards and to the right. (B) Centrin staining showing two distinct bodies (arrows) positioned at the anterior end of the cell. (C) Superimposed DIC and centrin-stained CLSM images showing the position of the two distinct bodies (arrows) along the edge of the anterior apparatus and just below the plasma membrane. (D) DIC image showing the central nucleus (N) and the ventral side of the cell as indicated by the anterior apparatus (bracket) oriented upwards and to the left. (E) Centrin staining showing two distinct bodies (arrows) positioned at the anterior end of the cell. (F) Superimposed DIC and centrin-stained CLSM images showing the position of the two distinct bodies (arrows) along the edge of the anterior apparatus and just below the plasma membrane. Scale bars: 20 μm.

mid-line of the trophozoites from the anterior apparatus to the posterior end (Figure 6). This row of stained points was evident in all focal planes of the observed trophozoites, demonstrating that each point represents a bundle of tubulin running through the cell from the ventral side to the dorsal side (i.e. perpendicular to the longitudinal bundles of microtubules) (Figure 6). Some of these "dorsoventral microtubule bundles" (DVMBs) were elongated in some focal planes, indicating areas where the cell was deformed in a way that angled the DVMBs relative to the dorsoventral axis of the cell (Figures 6 and 7A). Each trophozoite had between 15 and 20 DVMBs ($n = 15$), and the distance between the DVMBs ranged from 5 to 30 μm ($n = 20$). The trophozoites also had some scattered DVMBs located on the opposite side of the nucleus from the curved row of DVMBs; the number of these additional DVMBs ranged from 1 to 4 (Figure 6).

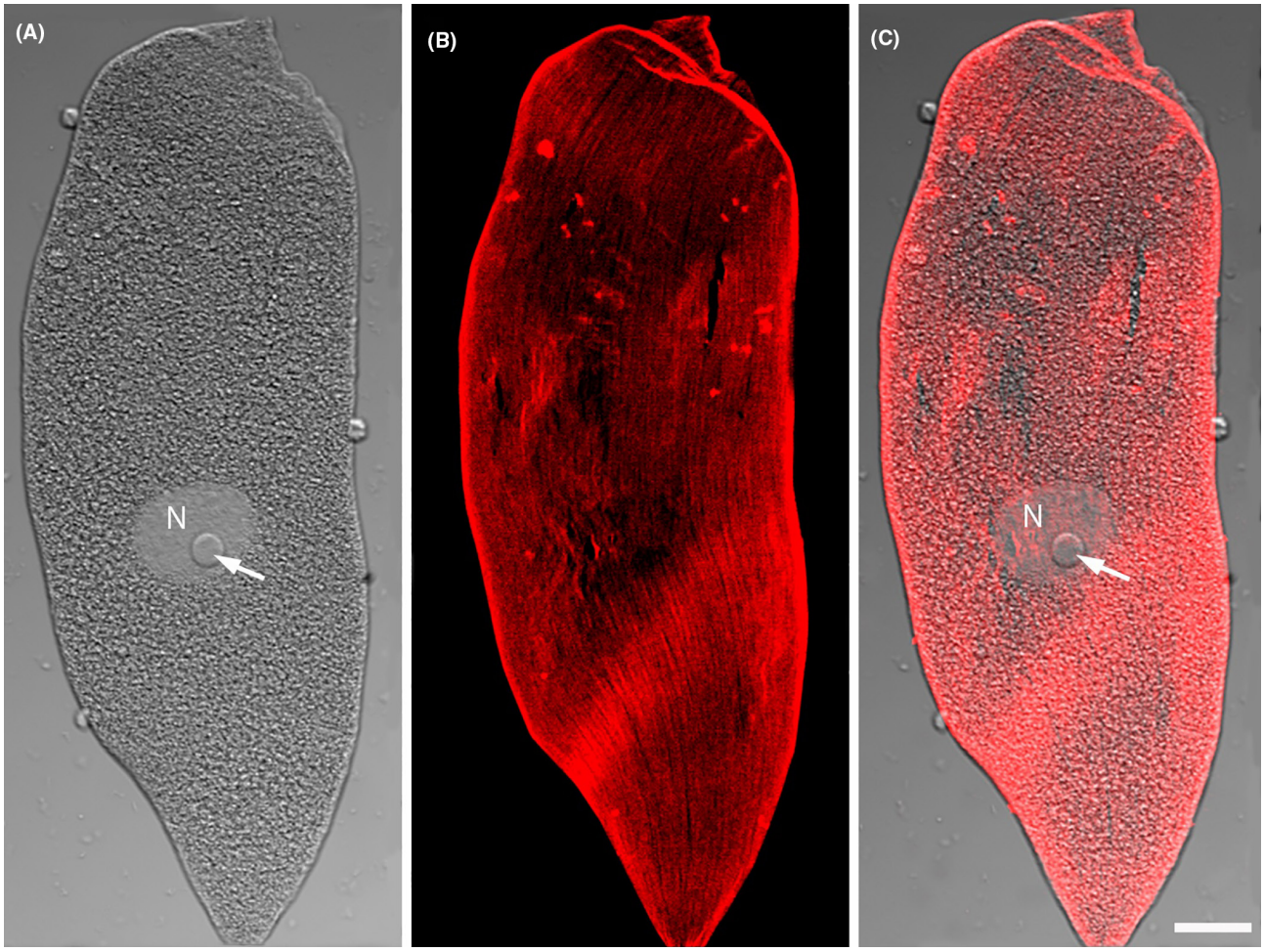

FIGURE 5 Confocal laser scanning micrographs (CLSM) of a trophozoite of *Platyproteum vivax* stained for alpha tubulin (red). (A) Differential interference contrast (DIC) light micrograph showing the dorsal surface of a trophozoite, nucleus (N), nucleolus (arrow), and anterior apparatus oriented upward and to the right. (B) Tubulin staining at a superficial focal plane showing the bundles of microtubules (red striations) running longitudinally along the entire length of the cell. (C) Superimposed DIC and tubulin-stained CLSM images showing the longitudinal microtubule bundles positioned beneath the dorsal surface of the cell. Scale bar: 20 μm.

Localization of mitochondria

MitoTracker staining on living trophozoites showed a continuous superficial layer of fluorescence that was 3–6 μm thick and localized below the plasma membrane (Figure 8). Mitochondrial staining was absent in deeper parts of the cell and within the inner-membrane complex that envelops the cell (Figure 9).

Localization of Actin

Phalloidin staining for F-actin did not reveal any patterns of fluorescence or localization in *P. vivax*.

DISCUSSION

Previous observations of the trophozoites in *P. vivax* have reported lengths ranging from 120 to 550 μm (Gunderson & Small, 1986; Leander, 2006; Leander & Keeling, 2003), which is consistent with the range reported in this study. The flattened shape and transverse surface striations combined with the dynamic peristaltic movements in *P. vivax* are inferred to facilitate surface-mediated nutrient uptake via endocytosis within the intestinal lumen of their host (Leander, 2006). TEM data from *P. vivax* demonstrated that the transverse surface striations are folded regions of the plasma membrane above the inner membrane complex that form during the dynamic changes in trophozoite shape (Leander, 2006). The trophozoites of some gregarines, especially species within *Selenidium*, also undergo dynamic undulating movements and produce similar transverse surface striations in contracted regions of the cell (Leander, 2006, 2007, 2008b; Paskerova et al., 2018; Schrével, 1970). These transverse striations occur over broad epicytic folds that run along the longitudinal axis of gregarine trophozoites (Leander, 2007). The number of longitudinal epicytic folds in different lineages of gregarines varies considerably (4 to >200), and higher numbers of epicytic

Journal of Eukaryotic Microbiology ISOP Published by the International Society of Protistologists

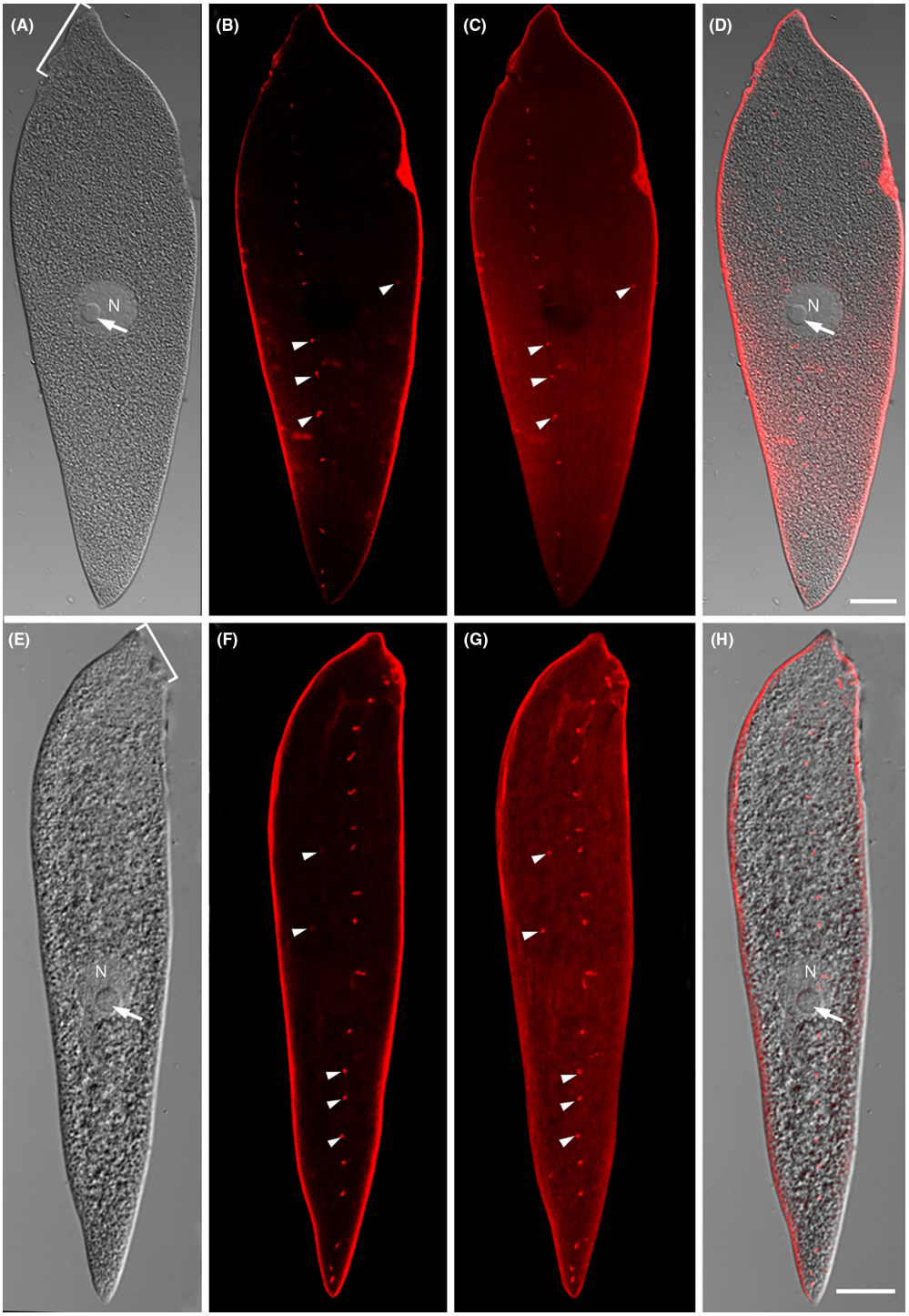

FIGURE 6 Confocal laser scanning micrographs (CLSM) of two different trophozoites of *Platyproteum vivax* stained for alpha tubulin (red). (A) Differential interference contrast (DIC) light micrograph showing a ventral view of a trophozoite, the nucleus (N), the nucleolus (arrow), and the anterior apparatus oriented upward and to the left (bracket). (B) Tubulin staining at a deeper focal plane showing a row of "dorsoventral microtubule bundles" (DVMBs, white arrowheads) running along the midline from the anterior apparatus to the posterior end of the cell. Some DVMBs (white arrowheads) are positioned outside of the distinct row of DVMBs on the opposite side of the cell. (C) Tubulin staining at a more superficial focal plane showing the same row of DVMBs (white single arrowheads). (D) Superimposed DIC and tubulin-stained CLSM images showing the same row of DVMBs passing to the left side of the nucleus when viewing the ventral side of the trophozoite. (E) DIC light micrograph showing a dorsal view of a trophozoite, the nucleus (N), the nucleolus (arrow), and the anterior apparatus oriented upward and to the right (bracket). (F) Tubulin staining at a deep focal plane showing a row of DVMBs (white arrowheads) running along the midline from the anterior apparatus to the posterior end of the cell. Some DVMBs (white arrowheads) are positioned outside of the distinct row of DVMBs on the opposite side of the cell. (G) Tubulin staining at a more superficial focal plane showing the same row of DVMBs (white arrowheads). (H) Superimposed DIC and tubulin-stained CLSM images showing the same row of DVMBs passing to the right side of the nucleus when viewing the dorsal side of the trophozoite. Scale bars: 20 μm.

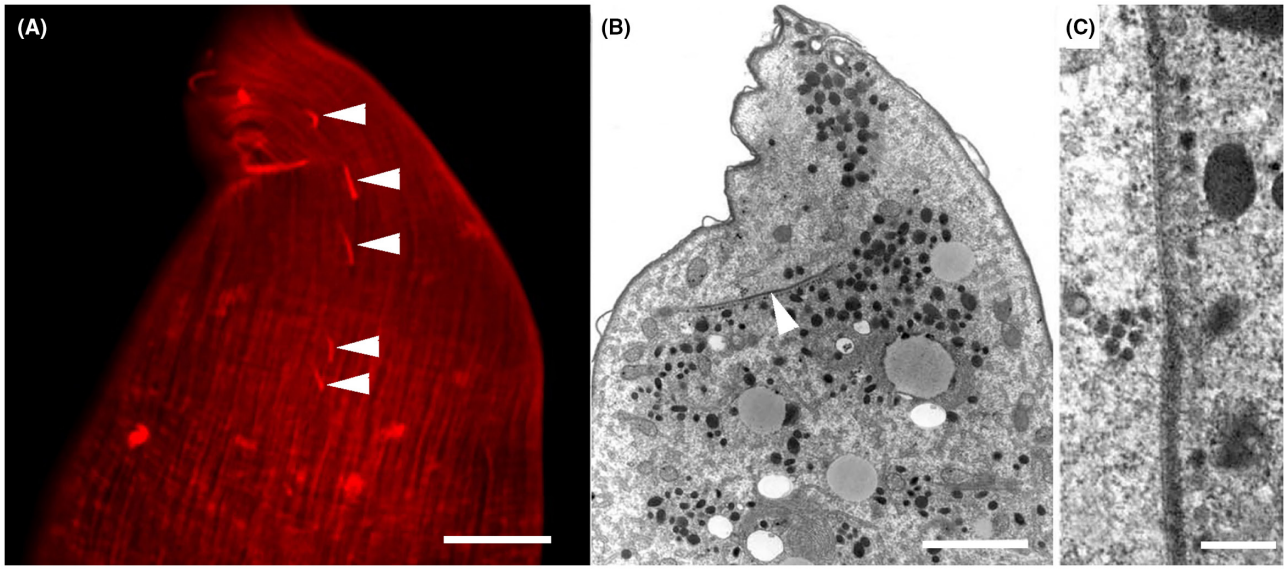

FIGURE 7 Transmission electron micrographs (TEM) and a confocal laser scanning micrograph (CLSM) of trophozoites of *Platyproteum vivax* stained for alpha tubulin (red) showing "dorsoventral microtubule bundles" (DVMBs). (A) High magnification CLSM of the anterior apparatus (oriented to the left) at a deep focal plane showing the linearity of several DVMBs (white arrowheads). Scale bar: 2 μm. (B) Low magnification TEM near the anterior apparatus of a trophozoite showing a linear thread (arrowhead) that is consistent with the ultrastructural position and form of the DVMBs observed with CLSM (modified with permission from Leander, 2006). Scale bar: 2 μm. (C) High magnification TEM of a putative DVMB (modified with permission from Leander, 2006). Scale bar: 0.25 μm.

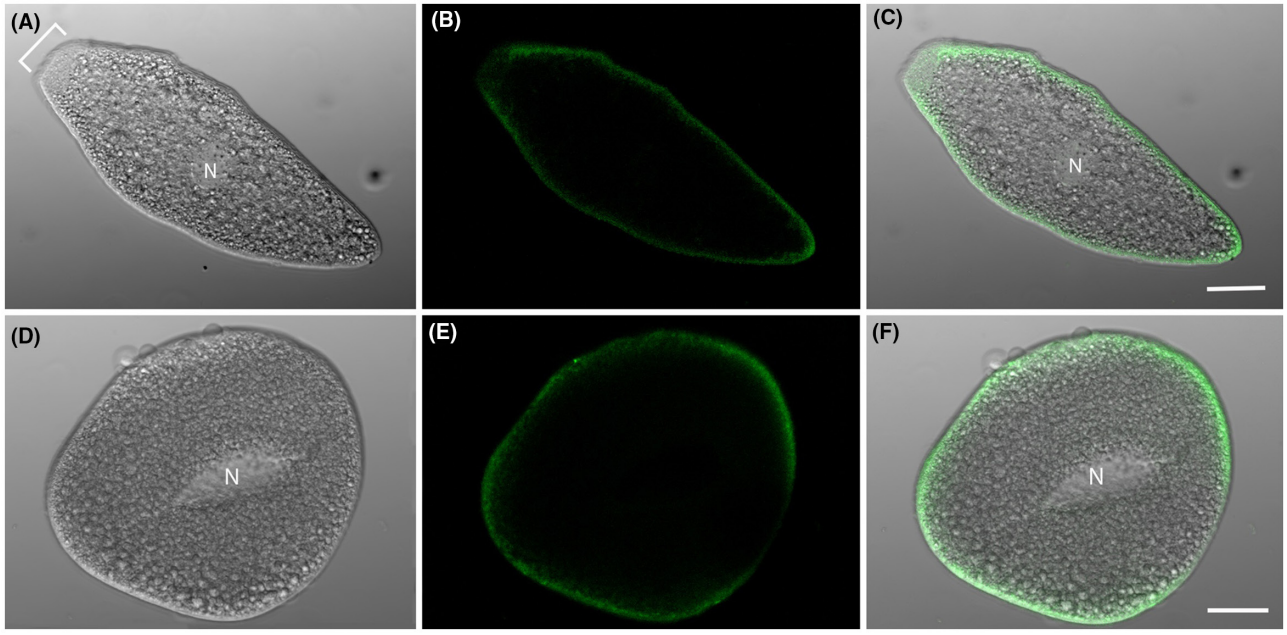

FIGURE 8 Confocal laser scanning micrographs (CLSM) of two different live trophozoites of *Platyproteum vivax* stained for mitochondria (green). (A, D) DIC images of each cell showing the anterior apparatus (bracket) and the nucleus (N). (B, E) Mitochondria staining shows a superficial layer of fluorescence that envelops the entire cell and the absence of fluorescence in the deeper regions of the cell. (C, F) Superimposed DIC and mitochondria-stained CLSM images showing the dense layer of fluorescence sitting below the inner-membrane complex and plasma membrane. Scale bars: 20 μm.

folds dramatically increase surface area for surface-mediated nutrition and gliding motility (Leander, 2007, 2008b; MacGregor & Thomas, 1965; Rueckert et al., 2019; Rueckert & Leander, 2009; Schrével, 1970; Simdyanov & Kuvardina, 2007; Yokouchi et al., 2022). However, molecular phylogenetic evidence has demonstrated that *Platyproteum* and *Selenidium* are only distantly related within the Myzozoa (Mathur et al., 2019) (Figure 1). Therefore, the presence of dynamic undulating movements and transverse surface striations in the

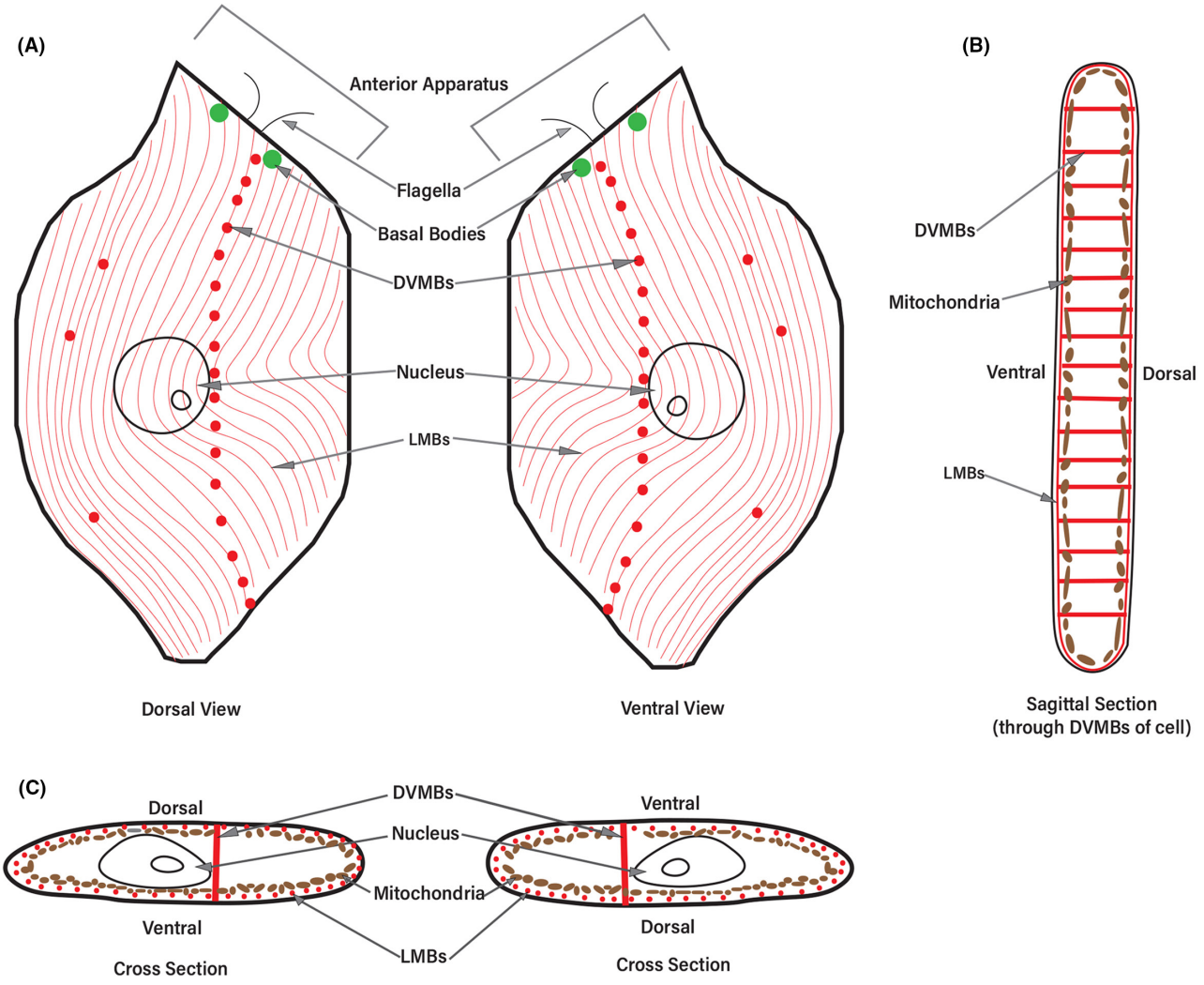

FIGURE 9 Illustrations summarizing the overall organization of microtubules, basal bodies, and mitochondria in the trophozoites of *Platyproteum vivax*. (A) Dorsal and ventral views of a trophozoite showing the anterior apparatus with two flagella oriented to the right and left, respectively. Green denotes the position of the basal bodies from which the flagella are derived. Red denotes microtubules. "Longitudinal microtubule bundles" (LMBs) are arranged in parallel along the entire anteroposterior axis of the cell, and "dorsoventral microtubule bundles" (DVMBs), indicated by red dots, are arranged perpendicular to the anteroposterior axis of the cell. Most of the DVMBs are aligned in a distinctive curved row that runs from the anterior to the posterior end of the trophozoite. The row of DVMBs is positioned to the right of the nucleus in dorsal view and to the left of the nucleus in ventral view. A few isolated DVMBs are scattered on the side of the nucleus opposite of the curved row of DVMBs. (B) Sagittal section showing the LMBs subtending the inner membrane complex and the perpendicular DVMBs running from the dorsal side to the ventral side of the trophozoite. Brown denotes the superficial layer of mitochondria located just above the LMB layer. (C) Cross sections through the nucleus of the trophozoite showing the LMBs subtending the inner membrane complex and a perpendicular DVMB running from the dorsal to ventral side of the cell.

trophozoites of these two lineages clearly reflect the convergent evolution of traits associated with acquiring nutrients within a similar habitat: the intestines of marine annelids.

The pair of flagella reported here on the trophozoites of *P. vivax* was also recently reported in another *Platyproteum* species collected off the coast of Japan, *P. noduliferae* (Yokouchi et al., 2022). These concordant findings explain the previous report of two unidentified "thread-like structures" emerging from pores on the anterior apparatus of the trophozoites in *P. vivax* (Leander, 2006). This previous report was unexpected because flagella were inferred to have been lost in the most recent ancestor of all apicomplexans, except in the male microgametes of some taxa (Adl et al., 2019; Cavalier-Smith, 2004; Moore et al., 2008; Nichols & Chiappino, 1987) (Figure 1). Therefore, the presence of two flagella in *Platyproteum* corroborates the molecular phylogenetic data that shows this lineage branching as the sister group of a clade consisting of bi-flagellated chrompodellids and un-flagellated apicomplexans (Mathur et al., 2019) (Figure 1).

Even though *P. vivax* can drastically change its cell shape, there is one feature that remains fairly constant:

the presence of a straight edge at the anterior end of the cell that reflects the extremely flattened shape of the trophozoites. A "mucron" refers to the anterior attachment apparatus in the trophozoites of gregarine apicomplexans. Although the shape and ornamentations of the mucron vary in different lineages of gregarines, the mucron is distinctively radially symmetrical (Mita et al., 2012; Rueckert et al., 2012, 2015, 2018; Wakeman, Heintzelman, & Leander, 2014; Wakeman & Leander, 2012; Wakeman, Reimer, et al., 2014). This fundamental difference in the anterior end of the trophozoites of *Platyproteum* and gregarines reflects the independent evolutionary origins of these two lineages in molecular phylogenetic analyses. Therefore, the term "mucron" is no longer applicable to describe the anterior end of *Platyproteum* and their relatives within the Squirmida, which is why we refer to it as the "anterior apparatus" instead.

The anterior apparatus of the intestinal parasite *Filipodium*, which is a close relative of *Platyproteum* found in the same host species, also takes on the form of a straight edge (Hoshide & Todd, 1992, 1996; Hukui, 1939; Rueckert & Leander, 2009; Tuzet & Ormieres, 1965). *Platyproteum noduliferae* was reported to have a more "hooked" attachment apparatus (Yokouchi et al., 2022). These reports show that even though there are variations in the form of the anterior apparatus within the Squirmida, the anterior end of the trophozoites in members of this clade are fundamentally different from the radially symmetrical mucrons of gregarines like *Selenidium* (Levine, 1971; Rueckert & Leander, 2009; Schrével, 1970; Simdyanov & Kuvardina, 2007) (Table 1).

Centrin, basal bodies and the flagellar apparatus

The trophozoites of both *P. vivax* and *P. noduliferae* have similar features that reflect their parasitic lifestyles within the intestines of sipunculids, such as highly flattened cells with dense arrays of transverse surface striations and rhythmic peristaltic movements (Leander, 2006; Yokouchi et al., 2022). However, the function of the two flagella in both species of *Platyproteum* is unclear. The flagella are tiny relative to the size of the trophozoites, so it is unlikely that the flagella are used to propel the cells through a liquid medium. Perhaps the flagella have a sensory function to help the trophozoites identify a suitable attachment site within the host intestine. The pores previously observed along the edge of the anterior apparatus in *P. vivax* could be involved in either the endocytosis of nutrients or the exocytosis of adhesive molecules for attachment (Leander, 2006). It is also possible that the surface area created by the highly flattened trophozoites allows them to adhere to the intestinal lining of their hosts by some unknown mechanism that does not involve the anterior apparatus at all. Nonetheless, it is clear that the presence of two flagella in the trophozoites of both *Platyproteum* species reflects an ancestral trait within the Myzozoa and distinguishes this lineage from all known apicomplexan parasites, especially gregarines (Table 1; Figure 1).

Two centrin-stained bodies were localized just below the plasma membrane of the anterior apparatus in the trophozoites of *P. vivax*. The position of these bodies within the anterior apparatus corresponded to the location of the two flagella in *P. vivax* and to the two basal bodies identified in the trophozoites of *P. noduliferae* (Yokouchi et al., 2022); this indicates that the centrin-stained areas in *P. vivax* are also basal bodies. The flagellar apparatus of *P. noduliferae* included the two basal bodies plus microtubule roots that were connected to fibrous material known as the root connective (Yokouchi et al., 2022). Previous studies of single-celled eukaryotes, such as green algae, ciliates, dinoflagellates, and retortamonads, have found that centrin is associated with connective fibers around the basal bodies (Beech et al., 1991; Beisson et al., 2001; Klotz et al., 1997; Levy et al., 1996; Okamoto & Keeling, 2014; Vaughan & Gull, 2015; Weerakoon et al., 1999). The distance between the centrin-stained bodies in *P. vivax*

TABLE 1 Comparison of traits in the trophozoites in *Platyproteum* (Squirmida) and *Selenidium* (Apicomplexa).

Trait	*Platyproteum*	*Selenidium*
Host type/environment	Invertebrate, marine	Invertebrate, marine
Host tissue	Intestine	Intestine
Cell shape	Tape-like, flattened	Spindle-shaped, vermiform
Anterior end	Straight-edge, hooked	Rounded, radially symmetrical
Epicytic longitudinal folds	No (transient)	Yes
Transverse folds	Yes	Yes
Movement	Twisting, undulating, folding	Twisting, undulating
Longitudinal microtubules	Yes	Yes
Dorsoventral microtubules	Yes	No
Two flagella	Yes	No

is greater than the distance between the two basal bodies in *P. noduliferae*, roughly 10 and 1 μm, respectively. This difference might reflect the much larger cell size of the trophozoites in *P. vivax* (e.g. over 500 μm long) compared to *P. noduliferae* (e.g. roughly 100 μm long), longer connecting fibers, or artifacts (e.g. cell squashing) introduced during the preparation of the cells for confocal laser scanning microscopy.

Organization of the tubulin-based cytoskeleton

The tubulin staining confirmed that loosely arranged bundles of microtubules subtend the plasma membrane and run longitudinally from the anterior to the posterior end of the trophozoites in *P. vivax* (Leander, 2006) (Figure 9). Movement of microtubules in a cell occurs by dynamic instability and through the forces generated by tubulin-associated ATP-driven motor proteins, such as dynein and kinesin (Guha et al., 2021; Tanenbaum et al., 2013). It has been inferred that the same mechanism is used to drive the undulating movements of trophozoites in *Selenidium* (Leander, 2007; Schrével, 1970) and the peristaltic movements in *Platyproteum* (Leander, 2006). The transverse striations on the surface of *Selenidium* and *Platyproteum* are indicative of the plasma membrane folding over on itself during the sliding of microtubules. This is consistent with the observation that there is a higher density of transverse surface striations on the more rounded, contracted regions of trophozoites than on elongated, relaxed regions. The dense superficial layer of mitochondria positioned just below the longitudinal microtubule bundles (LMBs) observed in both *P. vivax* and *P. noduliferae* likely supplies ATP to the motor proteins associated with the LMBs and therefore fuels the rhythmic cellular deformations (Leander, 2006; Yokouchi et al., 2022).

Tubulin staining also revealed a novel pattern of dorsoventral microtubule bundles (DVMBs) arranged in a curved row beginning at the anterior end of the cell and ending at the posterior end of the cell (Figure 9). This row of DVMBs was always situated to the right of the nucleus in dorsal view (i.e. when the anterior apparatus is oriented to the right) and to the left of the nucleus in ventral view (i.e. when the anterior apparatus is oriented to the left) (Figure 9). A few isolated DVMBs are scattered on the side of the nucleus opposite of the curved row of DVMBs. Because the DVMBs connect the LMBs on the dorsal side of the cell to the LMBs on the ventral side of the cell, they are likely involved in maintaining the flattened shape of the trophozoites during peristaltic movements. The DVMBs have the same orientation as the dorsoventral muscles in flatworms, which are involved in body flattening and in coordinating body shape changes (Brusca et al., 2022). Previous TEM data reported an "unidentified linear thread" near the anterior end of *P. vivax* that runs from the dorsal side of the cell to the ventral side of the cell, which corresponds exactly to the orientation of DVMBs when viewed with CLSM (see fig. 7D in Leander, 2006) (Figure 7). Higher-magnification TEMs show a uniform row of small electron-dense granules that run adjacent to the linear thread (see Figure 7D,F in Leander, 2006). A synthesis of the previous TEM data with the new CLSM data suggests that this previously unidentified linear thread is actually a tubulin-based DVMB. Currently, *P. vivax* is the only myzozoan known to have DVMBs, and the functional significance of this ultrastructural system appears to be a derived trait for this lineage and perhaps for its nearest relatives within the Squirmida.

Phalloidin did not stain Actin

Actin dynamics are associated with generating the forces necessary to produce dynamic cell shape changes and movements in a wide variety of eukaryotes (Etienne-Manneville, 2004). For instance, quick polymerization-depolymerization cycles between filamentous actin (F-actin) and globular actin (G-actin) combined with the actions of myosin motor proteins drive gliding motility in many apicomplexans (Soldati-Favre, 2008; Woo et al., 2015). Eugregarines (e.g. *Gregarina* spp.) have F-actin networks below the longitudinal epicytic folds, which facilitate gliding movements and control cell shape (Heintzelman, 2004; Valigurová et al., 2013). Therefore, the presence of F-actin and its possible role in cell movement in the trophozoites of *P. vivax* was investigated using the widely used fluorescently marked cyclic peptide phalloidin.

Filamentous actin in *P. vivax* was not stained by phalloidin (despite multiple attempts), so the organization of the actin-based cytoskeleton, if present, remains unclear. Interestingly, previous studies have shown that phalloidin also failed to bind to F-actin in several other apicomplexan genera, including *Gregarina* spp., *Toxoplasma* spp., and *Plasmodium* spp. (Heintzelman, 2004; Hirono et al., 1989; Shaw & Tilney, 1999). F-actin visualization in these groups was done by generating antibodies specific to the species being studied for immunolocalization or immunogold labeling with TEM. However, phalloidin binding has been successful in some eugregarine species, such as *Urospora travisiae* and *U. ovalis* (Valigurová et al., 2013, 2017), indicating that different lineages of apicomplexans express different families of F-actin. Molecular phylogenetic analyses suggest that apicomplexans have developed distinct properties in the highly conserved actin-binding proteins and have lost many of the actin-associated genes that chrompodellids possess (Morrissette, 2015; Woo et al., 2015). Considering

that *P. vivax* is more distantly related to apicomplexans than chrompodellids, there appear to have been several independent losses or major modifications of actin-associated genes within myzozoans. Nonetheless, *P. vivax* is similar to several other apicomplexan genera (e.g. *Gregarina*) in having F-actin populations that do not bind to phalloidin.

CONCLUSION

A more detailed investigation of the ultrastructure of *P. vivax* revealed novel traits that reflect the independent origins of *Platyproteum* and *Selenidium* within the intestines of marine invertebrates; this is consistent with phylogenomic data indicating that ultrastructural and behavioral similarities in the trophozoites of these two lineages arose by convergent evolution (Mathur et al., 2019). These similarities include trophozoites with vermiform cell shapes, dynamic undulating behavior, and robust layers of subpellicular microtubules originating from the anterior end of the cell (Leander, 2007; Schrével, 1971a, 1971b; Valigurová et al., 2017; Vivier & Schrével, 1964, 1966; Wakeman, Heintzelman, & Leander, 2014) (Table 1).

The flattened trophozoites in *Platyproteum* are also similar in shape, peristaltic behavior, and ultrastructure to the dorsoventrally flattened proglottids of tapeworms (Cestoda) (Leander, 2008a). Tapeworms have lost the gut of their ancestors and instead acquire nutrients within the host intestine using surface-mediated absorption (Arme, 1983; Brusca et al., 2022; Rueckert & Leander, 2009). The intestinal trophozoites of *Platyproteum* are inferred to acquire nutrients in the same way (Leander, 2006, 2008a). Both tapeworms and the trophozoites of *Platyproteum* have a superficial layer of mitochondria that reflects the low-oxygen conditions within the intestinal lumen of their host and that generates the ATP required to fuel endocytosis and the contraction of muscles and the sliding of LMBs, respectively. Moreover, the arrangement of LMBs and DVMBs in *P. vivax* is similar to the arrangement of longitudinal and dorsoventral muscles in flatworms (Platyhelminthes), which presumably help maintain the surface area created by the extremely flattened shape of *Platyproteum* trophozoites. Future studies using CLSM to investigate the ultrastructural systems of undescribed species of squirmids (e.g. *Filipodium*, *Platyproteum*, and novel genera) will determine whether any of the novel traits described in this study, such as a pair of inconspicuous flagella and a system of DVMBs are synapomorphic for the Squirmida as a whole or a subgroup therein.

AUTHOR CONTRIBUTIONS

BSL conceived, funded, and guided the study. DC-O conducted sampling and performed the microscopy within the context of her MSc research. DC-O and BSL built the figures and wrote the manuscript; DC-O and BSL made further revisions and approved the final version of the manuscript.

ACKNOWLEDGMENTS

A special thanks is owed to Dr. Eunji Park and Dr. Neils Van Steenkiste for their contributions to data collection. We thank staff members of the UBC Bioimaging Facility for advising on protocol development and assistance with image acquisition. Data collection and analysis for this project was conducted on the traditional, ancestral, and unceded territory of the xʷməθkʷəy̓əm (Musqueam) people. This work was funded by grants to BSL from the Hakai Institute and the National Sciences and Engineering Research Council of Canada (NSERC 2019-03986).

ORCID

Brian S. Leander https://orcid.org/0000-0003-0798-0470

REFERENCES

Adl, S.M., Bass, D., Lane, C.E., Lukes, J., Schoch, C.L., Smirnov, A. et al. (2019) Revisions to the classification, nomenclature, and diversity of eukaryotes. *Journal of Eukaryotic Microbiology*, 66, 4–119.

Angel, P., Herranz, M. & Leander, B.S. (2021) Insights into the morphology of haplozoan parasites (Dinoflagellata) using confocal laser scanning microscopy. *Journal of Eukaryotic Microbiology*, 68, e12855.

Arme, C. (1983) Aspects of tapeworm physiology. *Journal of Biological Education*, 17, 352–357.

Beech, P.L., Heimann, K. & Melkonian, M. (1991) Development of the flagellar apparatus during the cell cycle in unicellular algae. *Protoplasma*, 164, 23–37.

Beisson, J., Clérot, J.C., Fleury-Aubusson, A., Garreau de Loubresse, N., Ruiz, F. & Klotz, C. (2001) Basal body-associated nucleation center for the centrin based cortical cytoskeletal network in *Paramecium*. *Protist*, 152, 339–354.

Beisson, J. & Wright, M. (2003) Basal body/centriole assembly and continuity. *Current Opinion in Cell Biology*, 15, 96–104.

Brusca, R.C., Giribet, G. & Moore, W. (2022) *Invertebrates*, 4th edition, New York: Oxford University Press, pp. 527–554.

Bullen, H.E., Tonkin, C.J., O'Donnell, R.A., Tham, W.H., Papenfuss, A.T., Gould, S. et al. (2009) A novel family of apicomplexan glideosome-associated proteins with an inner membrane-anchoring role. *Journal of Biological Chemistry*, 284, 25353–25363.

Cavalier-Smith, T. (2004) Only six kingdoms of life. *Proceedings of the Royal Society B: Biological Sciences*, 271, 1251–1262.

Cavalier-Smith, T. (2014) Gregarine site-heterogeneous 18S rDNA trees, revision of gregarine higher classification, and the evolutionary diversification of Sporozoa. *European Journal of Protistology*, 50, 472–495.

Cavalier-Smith, T. & Chao, E.E. (2004) Protalveolate phylogeny and systematics and the origins of Sporozoa and dinoflagellates (phylum Myzozoa nom. nov.). *European Journal of Protistology*, 40, 185–212.

Desportes, I. & Schrével, J. (2013) Introduction: gregarines among Apicomplexa. In: *Treatise on Zoology-Anatomy, Taxonomy, Biology. The Gregarines*, Vol. 2, Netherlands: Brill Publishers, pp. 7–24.

Etienne-Manneville, S. (2004) Actin and microtubules in cell motility: which one is in control? *Traffic*, 5, 470–477.

Francia, M.E., Dubremetz, J.F. & Morrissette, N.S. (2015) Basal body structure and composition in the apicomplexans *Toxoplasma* and *Plasmodium*. *Cilia*, 5, 3.

Frénal, K., Dubremetz, J.F., Lebrun, M. & Soldati-Favre, D. (2017) Gliding motility powers invasion and egress in Apicomplexa. *Nature Reviews Microbiology*, 15, 645–660.

Guha, S., Patil, A., Muralidharan, H. & Baas, P.W. (2021) Mini-review: microtubule sliding in neurons. *Neuroscience Letters*, 753, 135867.

Gunderson, J. & Small, E.B. (1986) *Selenidium vivax* n. sp. (protozoa, Apicomplexa) from the sipunculid *Phascolosoma agassizii* Keferstein, 1867. *Journal of Parasitology*, 72, 107.

Heintzelman, M.B. (2004) Actin and myosin in *Gregarina polymorpha*. *Cell Motility and the Cytoskeleton*, 58, 83–95.

Heintzelman, M.B. (2015) Gliding motility in apicomplexan parasites. *Seminars in Cell and Developmental Biology*, 46, 135–142.

Hirono, M., Kumagai, Y., Numata, O. & Watanabe, Y. (1989) Purification of *Tetrahymena* Actin reveals some unusual properties. *Proceedings of the National Academy Sciences, USA*, 86, 75–79.

Höhfeld, I., Beech, P.L. & Melkonian, M. (1994) Immunolocalization of centrin in *Oxyrrhis marina* (Dinophyceae). *Journal of Phycology*, 30, 474–488.

Hoshide, K. & Todd, K.S. (1992) Structure and function of the mucron of *Filipodium ozakii* Hukui, 1939, (Apicomplexa, Gregarina). *Proceedings of the Zoological Society (Calcutta)*, 45, 53–59.

Hoshide, K. & Todd, K.S. (1996) The fine structure of cell surface and hair-like projections of *Filipodium ozakii* Hukui 1939 gamonts. *Acta Protozoologica*, 35, 309–315.

Hukui, T. (1939) On the gregarines from *Siphonosoma cumanense* (Keferstein). *Journal of Science of the Hiroshima University*, 7, 1–23.

Janouškovec, J., Paskerova, G.G., Miroliubova, T.S., Mikhailov, K.V., Birley, T., Aleoshin, V.V. et al. (2019) Apicomplexan-like parasites are polyphyletic and widely but selectively dependent on cryptic plastid organelles. *eLife*, 8, e49662.

Janouškovec, J., Tikhonenkov, D.V., Burki, F., Howe, A.T., Kolísko, M., Mylnikov, A.P. et al. (2015) Factors mediating plastid dependency and the origins of parasitism in apicomplexans and their close relatives. *Proceedings of the National Academy of Sciences of the United States of America*, 112, 10200–10207.

Kilburn, C. & Winey, M. (2008) Basal bodies. *Current Biology*, 18, R56–R57.

Klotz, C., Garreau de Loubresse, N., Ruiz, F. & Beisson, J. (1997) Genetic evidence for a role of centrin-associated proteins in the organization and dynamics of the infraciliary lattice in *paramecium*. *Cell Motility and the Cytoskeleton*, 38, 172–186.

Kuvardina, O.N., Leander, B.S., Aleshin, V.V., Myl'nikov, A.P., Keeling, P.J. & Simdyanov, T.G. (2002) The phylogeny of colpodellids (Alveolata) using small subunit rRNA gene sequences suggests they are the free-living sister group to apicomplexans. *Journal of Eukaryotic Microbiology*, 49, 498–504.

Leander, B.S. (2006) Ultrastructure of the archigregarine *Selenidium vivax* (Apicomplexa) — a dynamic parasite of sipunculid worms (host: *Phascolosoma agassizii*). *Marine Biology Research*, 2, 178–190.

Leander, B.S. (2007) Molecular phylogeny and ultrastructure of *Selenidium serpulae* (Apicomplexa, Archigregarinia) from the calcareous tubeworm *Serpula vermicularis* (Annelida, polychaeta, Sabellida). *Zoologica Scripta*, 36, 213–227.

Leander, B.S. (2008a) A hierarchical view of convergent evolution in microbial eukaryotes. *Journal of Eukaryotic Microbiology*, 55, 59–68.

Leander, B.S. (2008b) Marine gregarines: evolutionary prelude to the apicomplexan radiation? *Trends in Parasitology*, 24, 60–67.

Leander, B.S., Harper, J.T. & Keeling, P.J. (2003) Molecular phylogeny and surface morphology of marine aseptate gregarines (Apicomplexa): *Selenidium* and *Lecudina*. *Journal of Parasitology*, 89, 1191–1205.

Leander, B.S. & Keeling, P.J. (2003) Morphostasis in alveolate evolution. *Trends in Ecology & Evolution*, 18, 395–402.

Levine, N.D. (1971) Taxonomy of Archigregarinorida and Selenidiidae (Protozoa, Apicomplexa). *Journal of Protozoology*, 18, 704–717.

Levy, Y.Y., Lai, E.Y., Remillard, S.P., Heintzelman, M.B. & Fulton, C. (1996) Centrin is a conserved protein that forms diverse associations with centrioles and MTOCs in *Naegleria* and other organisms. *Cell Motility and the Cytoskeleton*, 33, 298–323.

MacGregor, H.C. & Thomas, P.A. (1965) The fine structure of two archigregarines, *Selenidium fallax* and *Ditrypanocystis cirratuli*. *Journal of Protozoology*, 12, 438–443.

Marshall, W.F. (2008) Basal bodies: platforms for building cilia. *Current Topics in Developmental Biology*, 85, 1–22.

Mathur, V., Kolísko, M., Hehenberger, E., Irwin, N.A., Leander, B.S., Kristmundsson, A. et al. (2019) Multiple independent origins of apicomplexan-like parasites. *Current Biology*, 29, 2936.e5–2936.e2941.

Mita, K., Kawai, N., Rueckert, S. & Sasakura, Y. (2012) Large-scale infection of the ascidian *Ciona intestinalis* by the gregarine *Lankesteria ascidiae* in an inland culture system. *Diseases of Aquatic Organisms*, 101, 185–195.

Moestrup, Ø. (2000) The flagellate cytoskeleton: introduction of a general terminology for microtubular flagellar roots in protists. In: Green, J.C. & Leadbeater, B.S.C. (Eds.) *The flagellates: unity, diversity and evolution*. London: Taylor and Francis.

Moore, R.B., Oborník, M., Janouškovec, J., Chrudimsky, T., Vancova, M., Green, D.H. et al. (2008) A photosynthetic alveolate closely related to apicomplexan parasites. *Nature*, 451, 959–963.

Morrissette, N. (2015) Targeting *Toxoplasma* tubules: tubulin, microtubules, and associated proteins in a human pathogen. *The Eukaryotic Cell*, 14, 2–12.

Morrissette, N.S., Murray, J.M. & Roos, D.S. (1997) Subpellicular microtubules associate with an intramembranous particle lattice in the protozoan parasite *Toxoplasma gondii*. *Journal of Cell Science*, 110, 35–42.

Mylnikov, A.P. (2009) Ultrastructure and phylogeny of colpodellids (Colpodellida, Alveolata). *Biological Bulletin*, 36, 582–590.

Nichols, B.A. & Chiappino, M.L. (1987) Cytoskeleton of *Toxoplasma gondii*. *Journal of Protozoology*, 34, 217–226.

Okamoto, N. & Keeling, P.J. (2014) The 3D structure of the apical complex and association with the flagellar apparatus revealed by serial TEM tomography in *Psammosa pacifica*, a distant relative of the Apicomplexa. *PLoS One*, 9, e84653.

Pacheco, N.D.S., Tosetti, N., Koreny, L., Waller, R.F. & Soldati-Favre, D. (2020) Evolution, composition, assembly, and function of the conoid in Apicomplexa. *Trends in Parasitology*, 36, 688–704.

Paskerova, G.G., Miroliubova, T.S., Diakin, A., Kováčiková, M., Valigurová, A., Guillou, L. et al. (2018) Fine structure and molecular phylogenetic position of two marine gregarines, *Selenidium pygospionis* sp. n. and *S. Pherusae* sp. n., with notes on the phylogeny of Archigregarinida (Apicomplexa). *Protist*, 169, 826–852.

Portman, N. & Šlapeta, J. (2014) The flagellar contribution to the apical complex: a new tool for the eukaryotic Swiss army knife? *Trends in Parasitology*, 30, 58–64.

Roberts, K.R. & Roberts, J.E. (1991) The flagellar apparatus and cytoskeleton of the dinoflagellates: a comparative overview. *Protoplasma*, 164, 105–122.

Rueckert, S., Betts, E.L. & Tsaousis, A.D. (2019) The symbiotic spectrum: where do the gregarines fit? *Trends in Parasitology*, 35, 687–694.

Rueckert, S., Glasinovich, N., Diez, M.E., Cremonte, F. & Vázquez, N. (2018) Morphology and molecular systematic of marine gregarines (Apicomplexa) from southwestern Atlantic spionid polychaetes. *Journal of Invertebrate Pathology*, 159, 49–60.

Rueckert, S. & Leander, B.S. (2009) Molecular phylogeny and surface morphology of marine archigregarines (Apicomplexa),

Selenidium spp., *Filipodium phascolosomae* n. sp., and *Platyproteum* n. g. and comb. from north-eastern Pacific peanut worms (Sipuncula). *Journal of Eukaryotic Microbiology*, 56, 428–439.

Rueckert, S., Wakeman, K.C., Jenke-Kodama, H. & Leander, B.S. (2015) Molecular systematics of marine gregarine apicomplexans from Pacific tunicates, with descriptions of five novel species of *Lankesteria*. *International Journal of Systematic and Evolutionary Microbiology*, 65, 2598–2614.

Rueckert, S., Wakeman, K.C. & Leander, B.S. (2012) Discovery of a diverse clade of gregarine apicomplexans (Apicomplexa: Eugregarinorida) from Pacific eunicid and onuphid polychaetes, including descriptions of *Paralecudina* n. gen., *Trichotokara japonica* n. sp., and *T. eunicae* n. sp. *Journal of Eukaryotic Microbiology*, 60, 121–136.

Ruiz, F., Garreau de Loubresse, N., Klotz, C., Beisson, J. & Koll, F. (2005) Centrin deficiency in *Paramecium* affects the geometry of basal-body duplication. *Current Biology*, 15, 2097–2106.

Salisbury, J.L. (1995) Centrin, centrosomes, and mitotic spindle poles. *Current Opinion in Cell Biology*, 7, 39–45.

Salisbury, J.L., Baron, A.T., Surek, B. & Melkonian, M. (1984) Striated flagellar roots: isolation and partial characterization of a calcium-modulated contractile organelle. *Journal of Cell Biology*, 99, 962–970.

Schrével, J. (1970) Contribution a parasites d'annelides polychetes. I. Cycles. *Protistologica*, 6, 389–426.

Schrével, J. (1971a) Observations biologique et ultrastructurales sur les Selenidiidae et leurs conséquences sur la systematique des gregarinomorphes. *Journal of Protozoology*, 18, 448–470.

Schrével, J. (1971b) Contribution a l'etude des Selenidiidae parasites d'annélides polychetes. II. Ultrastructure de quelques trophozoites. *Protistologica*, 7, 101–130

Shaw, M.K. & Tilney, L.G. (1999) Induction of an acrosomal process in *Toxoplasma gondii*: visualization of Actin filaments in a protozoan parasite. *Proceedings of the National Academy of Sciences of the United States of America*, 96, 9095–9099.

Simdyanov, T.G. & Kuvardina, O.N. (2007) Fine structure and putative feeding mechanism of the archigregarine *Selenidium orientale* (Apicomplexa: Gregarinomorpha). *European Journal of Protistology*, 43, 17–25.

Soldati-Favre, D. (2008) Molecular dissection of host cell invasion by the apicomplexans: the glideosome. *Parasite*, 15, 197–205.

Tanenbaum, M.E., Vale, R.D. & McKenney, R.J. (2013) Cytoplasmic dynein crosslinks and slides anti-parallel microtubules using its two motor domains. *eLife*, 2, e0094.

Tuzet, O. & Ormieres, R. (1965) Sur quelques gregarines parasites de phascolion et aspidosiphon (Sipunculiens). *Protistologica*, 1, 43–48.

Valigurová, A., Vaškovicová, N., Diakin, A., Paskerova, G.G., Simdyanov, T.G. & Kováčiková, M. (2017) Motility in blastogregarines (Apicomplexa): native and drug-induced organisation of *Siedleckia nematoides* cytoskeletal elements. *PLoS One*, 12, e0179709.

Valigurová, A., Vaškovicová, N., Musilová, N. & Schrével, J. (2013) The enigma of eugregarine epicytic folds: where gliding motility originates? *Frontiers in Zoology*, 10, 57.

Vaughan, S. & Gull, K. (2015) Basal body structure and cell cycle-dependent biogenesis in *Trypanosoma brucei*. *Cilia*, 5, 1–7.

Vivier, E. & Schrével, J. (1964) Étude, au microscope électronique, d'une grégarine du genre *Selenidium*, parasite de *Sabellaria alveolata*. *Journal de Microscopie*, 3, 651–670.

Vivier, E. & Schrével, J. (1966) Les ultrastructures cytoplasmiquesde *Selenidium hollandei*, n. sp. grégarine parasite de *Sabellaria alveolata* L. *Journal de Microscopie*, 5, 213–228.

Wakeman, K.C., Heintzelman, M.B. & Leander, B.S. (2014) Comparative ultrastructure and molecular phylogeny of *Selenidium melongena* n. sp. and *S. terebellae* ray 1930 demonstrate niche partitioning in marine gregarine parasites (Apicomplexa). *Protist*, 165, 493–511.

Wakeman, K.C. & Horiguchi, T. (2018) Morphology and molecular phylogeny of the marine gregarine parasite *Selenidium oshoroense* n. sp. (Gregarina, Apicomplexa) isolated from a Northwest Pacific *Hydroides ezoensis* Okuda 1934 (Serpulidae, polychaeta). *Marine Biodiversity*, 48, 1489–1498.

Wakeman, K.C. & Leander, B.S. (2012) Molecular phylogeny of Pacific archigregarines (Apicomplexa), including descriptions of *Veloxidium leptosynaptae* n. gen., n. sp., from the sea cucumber *Leptosynapta clarki* (Echinodermata), and two new species of *Selenidium*. *Journal of Eukaryotic Microbiology*, 59, 232–245.

Wakeman, K.C., Reimer, J.D., Jenke-Kodama, H. & Leander, B.S. (2014) Molecular phylogeny and ultrastructure of *Caliculium glossobalani* n. gen. et sp. (Apicomplexa) from a Pacific *Glossobalanus minutus* (Hemichordata) confounds the relationships between marine and terrestrial gregarines. *The Journal of Eukaryotic Microbiology*, 61, 343–353.

Weerakoon, N.D., Harper, J.D.I., Simpson, A.G.B. & Patterson, D.J. (1999) Centrin in the groove: immunolocalisation of centrin and microtubules in the putatively primitive protist *Chilomastix cuspidata* (Retortmonadida). *Protoplasma*, 210, 75–84.

Woo, Y.H., Ansari, H., Otto, T.D., Klinger, C.M., Kolísko, M., Michalek, J. et al. (2015) Chromerid genomes reveal the evolutionary path from photosynthetic algae to obligate intracellular parasites. *eLife*, 4, e06974.

Yokouchi, K., Iritani, D., Lim, K.H., Phua, Y.H., Horiguchi, T. & Wakeman, K.C. (2022) Description of an enigmatic alveolate, *Platyproteum noduliferae* n. sp., and reconstruction of its flagellar apparatus. *Protist*, 173, 125878.

Yubuki, N., Cepicka, I. & Leander, B.S. (2016) Evolution of the microtubular cytoskeleton (flagellar apparatus) in parasitic protists. *Molecular and Biochemical Parasitology*, 209, 26–34.

Yubuki, N. & Leander, B.S. (2013) Evolution of microtubule organizing centers across the tree of eukaryotes. *The Plant Journal*, 75, 230–244.

How to cite this article: Currie-Olsen, D. & Leander, B.S. (2024) Novel cytoskeletal traits in the intestinal parasites (Squirmida, *Platyproteum vivax*) of Pacific peanut worms (Sipuncula, *Phascolosoma agassizii*). *Journal of Eukaryotic Microbiology*, 71, e13023. Available from: https://doi.org/10.1111/jeu.13023